Measuring the critical resolved shear stresses in Mg alloys by instrumented nanoindentation

R. Sánchez-Martín , M.T. Pérez-Prado , J. Segurado , J. Bohlen , I. Gutiérrez-Urrutia , J. Llorca , J.M. Molina-Aldareguia

Abstract

One of the main limiting factors in the development of new magnesium (Mg) alloys with enhanced mechanical behavior is the need to use vast experimental campaigns for microstructure and property screening. For example, the influence of new alloying additions on the critical resolved shear stresses (CRSSs) is currently evaluated by a combination of macroscopic single-crystal experiments and crystal plasticity finite-element simulations (CPFEM). This time-consuming process could be considerably simplified by the introduction of high-throughput techniques for efficient property testing. The aim of this paper is to propose a new and fast, methodology for the estimation of the CRSSs of hexagonal close-packed metals which, moreover, requires small amounts of material. The proposed method, which combines instrumented nanoindentation and CPFEM modeling, determines CRSS values by comparison of the variation of hardness (H) for different grain orientations with the outcome of CPFEM. This novel approach has been validated in a rolled and annealed pure Mg sheet, whose H variation with grain orientation has been successfully predicted using a set of CRSSs taken from recent crystal plasticity simulations of single-crystal experiments. Moreover, the proposed methodology has been utilized to infer the effect of the alloying elements of an MN11 (Mg–1% Mn–1% Nd) alloy. The results support the hypothesis that selected rare earth intermetallic precipitates help to bring the CRSS values of basal and non-basal slip systems closer together, thus contributing to the reduced plastic anisotropy observed in these alloys.

Keywords: Nanoindentation; Crystal plasticity modeling; Critical resolved shear stresses; Rare earths; Magnesium alloys

1. Introduction

Weight reduction is a cost-effective approach to decrease fossil fuel consumption and greenhouse gas emissions in transport. Magnesium (Mg), the lightest structural metal, and its alloys, offer many possibilities in this direction. However, progress is still needed on alloy development in order to meet industrial needs and facilitate a wider commercialization of these materials [1,2].

An important limitation of wrought (rolled and extruded) Mg alloys is their inherent strong mechanical anisotropy, a consequence of their hexagonal closed-packed (hcp) lattice. Several reasons contribute to this effect. First, at room temperature, the critical resolved shear stresses (CRSSs) of basal and non-basal slip systems have very different values, spanning several orders of magnitude (Table 1) [3–10]; second, twinning, a very common

Table 1
CRSS values proposed for pure Mg.

Method	CRSS (MPa)		
	Basal ⟨a⟩	Prismatic ⟨a⟩	Pyramidal ⟨c+a⟩
Single-crystal [3]	0.81		
Single-crystal [4]	0.76		
Single-crystal [5]	0.52		
Single-crystal [6]		39	
Single-crystal [7]		50	
Single-crystal (micropillar) [8]			44
Single-crystal and polycrystal CP model [9]	1	20	40
Single-crystal and polycrystal CP model [10]	0.5	25	40

deformation mechanism in these materials, exhibits a pronounced polarity, i.e. its activation is dependent on the relative orientation between the *c*-axis and the applied stress [11]; finally, both hot and cold deformation processing textures are often quite sharp [12–16]. Together, these factors lead to a dependence of the dominant deformation mechanisms on the testing mode (tension or compression) and on the testing direction, resulting in large differences in yield stress values and strain-hardening responses [17–19]. One promising strategy to improve the mechanical behavior of Mg alloys relies on the design of new alloy compositions. For instance, alloying with rare earth (RE) elements greatly reduces the mechanical anisotropy of Mg alloys mainly due to two reasons, namely the weakening of hot processing texture [20–22], and the balancing of the CRSSs of the different slip systems [23–25]. As a result, the tension/compression asymmetry in the yield stress decreases dramatically with RE additions, even becoming negligible in some cases [23].

Current strategies for the development of new Mg alloys rely mostly on trial-and-error experimental approaches that are costly and time consuming. Novel computational techniques are thus required, capable of predicting the mechanical behavior of complex Mg alloys as a function of texture and processing conditions [26]. In this context, crystal plasticity (CP) models [9,10,27,28] are very valuable for quantifying the complex relationship between the plasticity at the single-crystal level, through the CRSSs of the different slip systems, and macroscopic properties such as yield stress and/or strain hardening.

Calibration of CP models requires the estimation of the CRSSs of the different slip systems, which are not easy to obtain experimentally. Currently, this task is performed by either testing single crystals in different crystallographic directions [3–7,29,30] or by fitting the mechanical behavior of polycrystalline aggregates with varying textures and/or under different loading conditions [9,10,28,31–33]. Both approaches are time consuming and costly. In the first instance they require the fabrication of large single crystals. In the former method, the results obtained are very sensitive to the approaches taken in the fitting procedure and it is not infrequent that different authors report different (or even contradictory) values for similar materials. These problems in the objectivity of the crystal properties obtained can be alleviated by using an appropriate optimization procedure as proposed in Ref. [33]. However, even in this case, a large battery of mechanical tests under different loading conditions is needed for accurate results. For these reasons, neither approach can be used as a quick evaluator of the effect of multiple alloying additions on the CRSSs in the context of the development of new Mg alloys.

The recent progress in the development of novel nanomechanical testing methods has opened a new door in polycrystal plasticity by using very small testing volumes, and hence reducing by many orders of magnitude both the volume of material and the time required compared to conventional macroscopic testing techniques. The most widespread nanomechanical testing method is instrumented nanoindentation, in which hardness is measured by making a small imprint on the surface of the material with the help of a hard indenter, typically of pyramidal or conical geometry. Imprints can be made sufficiently small to fit a number inside a single grain, even for grains as small as 1 μm. The indentation response mainly depends on the crystallographic orientation of the grain, and thus this information can potentially be used to calibrate the CRSSs of a CP model. However, the complex stress state that develops under indentation, together with the so-called indentation size effect (ISE), have so far prevented the use of this approach.

In this work, we aim at overcoming this problem by carrying out a coupled experimental and CPFEM study of the nanoindentation of Mg single crystals as a function of crystallographic orientation. In particular, we show that the variation of hardness with respect to the orientation of the grain (measured through the angle between the indentation axis and the *c*-axis of the crystal, referred to as the declination angle of the grain, see Fig. 1), follows a characteristic behavior than can be rationalized as a function of the ratios of the CRSSs of the different slip systems, i.e. basal, prismatic and pyramidal. Based on this result, we propose a novel and efficient methodology to estimate the CRSSs of Mg and its alloys, combining instrumented nanoindentation and CPFEM simulations. The proposed methodology requires only a small amount of material, allowing for the fast screening of several alloying addition combinations. The approach is calibrated on pure Mg using CRSSs values obtained from the literature. We apply

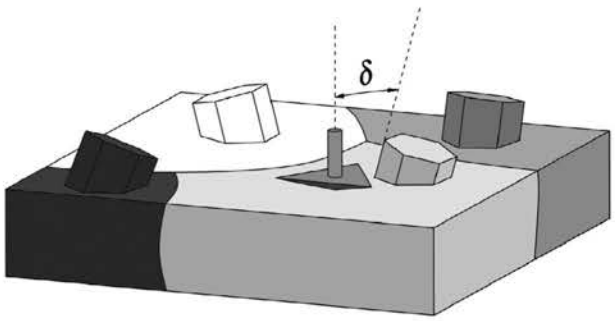

Fig. 1. Schematic representation of the declination angle (δ).

this approach to the investigation of the influence of Nd alloying additions on the CRSSs of the different slip systems in a RE MN11 alloy.

2. Experimental procedure

The materials studied in this work are an annealed rolled sheet of pure Mg and an extruded bar of the MN11 Mg alloy. The Mg sheet has equiaxed grains, ~100 μm in size, and a strong basal texture (Fig. 2), typical of rolled Mg sheets [34]. The MN11 alloy has a much more refined microstructure (Fig. 3) with a mean grain size of 10 μm, and shows a relatively weak texture, typical of Mg alloys containing RE elements [20–22].

Microstructure characterization was evaluated by electron backscatter diffraction (EBSD) using a 6500 F JEOL field emission gun-scanning electron microscope equipped with an EDAX/TSL OIM EBSD system. EBSD maps were performed at 15 kV using a step size ranging between 1 μm (MN11 alloy) and 10 μm (pure Mg). The limits of the areas mapped by EBSD were marked by Vickers microindentation in order to identify them in the nanoindentation test. Sample preparation for EBSD examination consisted, first, of cutting discs ~3 mm thick and 17 mm in diameter followed by surface grinding to 2000 grit and polishing with 1 μm diamond paste. Finally, samples were electropolished using a Struers AC2 solution cooled to 5 °C, applying a voltage of 20 V for 45 s.

Based on the EBSD maps, individual grains with different declination angles (δ) were indented in both materials using a Hysitron TI950 triboindenter equipped with feedback control and a Berkovich tip. Grain boundary effects were avoided by placing the indents in the middle of grains and using an indentation depth as small as 300 nm. Indentations were carried out in displacement control using a trapezoidal loading curve, with a loading and unloading time of 5 s, and a 2 s hold time at maximum depth. Hardness values were computed from the loading–unloading curves by applying the Oliver and Pharr method [35]. Due to the relatively small grain size of the MN11 alloy, the locations of the indents were examined by a Zeiss EVO MA15 scanning electron microscope to ensure that grain boundary effects are negligible in the present study.

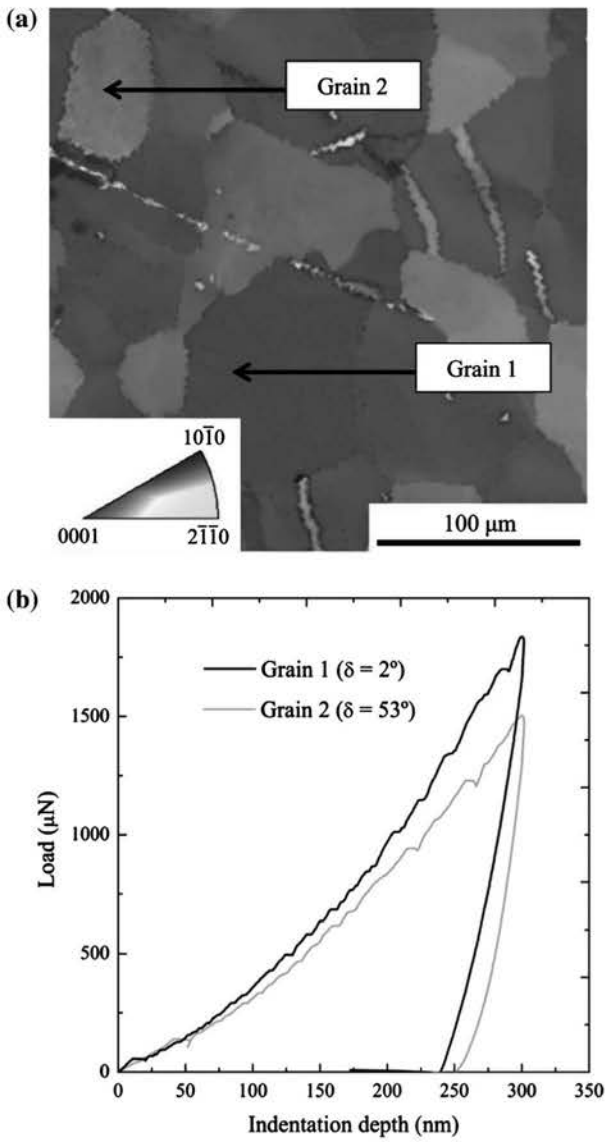

Fig. 2. (a) EBSD inverse pole figure map in the normal direction (ND) of pure Mg. (b) Effect of the declination angle on the load–displacement indentation curve in pure Mg.

3. Numerical simulations

3.1. Brief description of the crystal plasticity model

A standard CP model [27] was used to simulate the plastic behavior of the Mg alloys taking into account their hcp crystallographic structure. The model relies on the multiplicative decomposition of the deformation gradient [36], $\boldsymbol{F}$, into the elastic, $\boldsymbol{F}^e$, and plastic part, $\boldsymbol{F}^p$, following the expression:

$$\boldsymbol{F} = \boldsymbol{F}^e \boldsymbol{F}^p, \tag{1}$$

where $\boldsymbol{F}^p$ correspond to the so-called relaxed configuration.

Taking into account the definition of velocity gradient, $\boldsymbol{L}$, expression (1) leads to:

$$\boldsymbol{L} = \dot{\boldsymbol{F}}\boldsymbol{F}^{-1} = \boldsymbol{F}^e \dot{\boldsymbol{F}}^{e-1} + \boldsymbol{F}^e \dot{\boldsymbol{F}}^p \boldsymbol{F}^{p-1} \boldsymbol{F}^{e-1}, \tag{2}$$

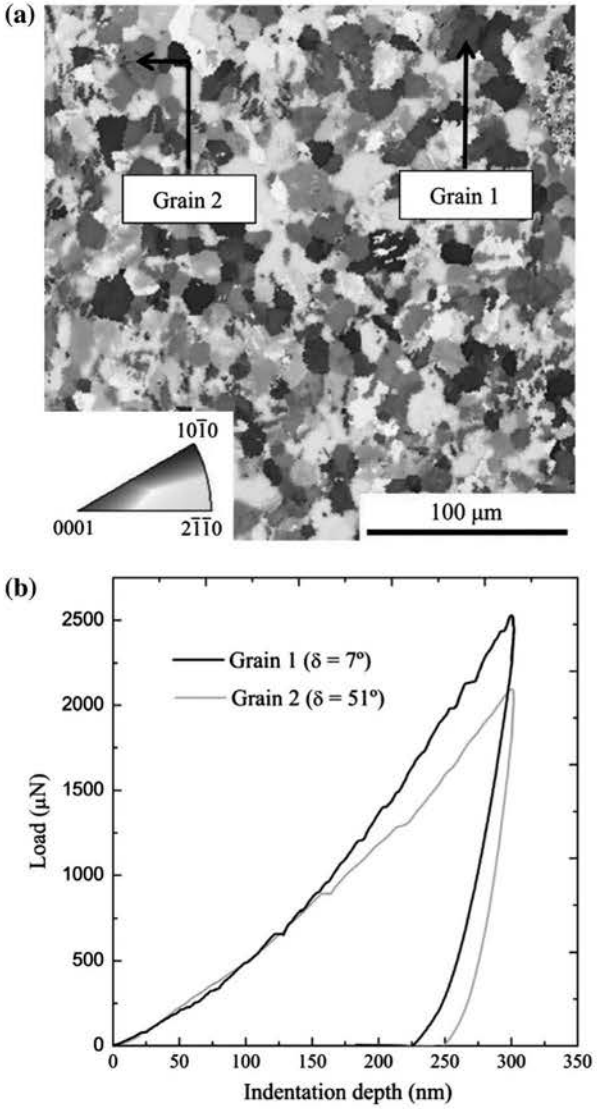

Fig. 3. (a) EBSD inverse pole figure map in the extrusion direction (ED) of the MN11 alloy. (b) Effect of the declination angle on the load–displacement indentation curve in the MN11 alloy.

where $\boldsymbol{L}^p = \dot{\boldsymbol{F}}^p \boldsymbol{F}^{p-1}$ is the plastic-velocity gradient, corresponding to the intermediate configuration.

As the plastic deformation is defined by the glide on the different slip systems, $\boldsymbol{L_p}$ is calculated by the sum of the shear rates, $\dot{\gamma}^\alpha$, of each slip system, α, as:

$$\boldsymbol{L}^p = \sum_\alpha \dot{\gamma}^\alpha \boldsymbol{s}^\alpha \otimes \boldsymbol{m}^\alpha, \tag{3}$$

were $\boldsymbol{s}^\alpha$ and $\boldsymbol{m}^\alpha$ stand for the unit vectors in the slip direction and perpendicular to the slip plane, respectively.

The plastic behavior of the crystal, $\dot{\gamma}^\alpha$, is modeled following a viscoplastic law [37,38] as a function of the resolved shear stresses, τ^α:

$$\dot{\gamma}^\alpha = \dot{\gamma}_0 \left(\frac{|\tau^\alpha|}{g^\alpha} \right)^{\frac{1}{m}} sing(\tau^\alpha), \tag{4}$$

where $\dot{\gamma}_0$ and m are the reference shear strain rate and the rate-sensitive exponent [39], respectively. The evolution of the slip resistance, g^α, depends on the shear rates, $\dot{\gamma}^\beta$, according to the following expression:

$$\dot{g}^\alpha = \sum_\beta q_{\alpha\beta} h(\Gamma) \dot{\gamma}_\beta, \tag{5}$$

where $q_{\alpha\beta}$ with $\alpha = \beta$ and $\alpha \neq \beta$ are the self-hardening and latent hardening coefficients, respectively. The hardening modulus, $h(\Gamma)$, follows the phenomenological expression given by Assaro and Needleman [38]:

$$h(\Gamma) = h_0 sech \left| \frac{h_0 \Gamma}{\tau_s - \tau_0} \right|^2, \tag{6}$$

where h_0 is the initial hardening modulus and τ_0 and τ_s are the initial and saturation yield stress, respectively. The accumulated shear strain in all the slip systems is given by:

$$\Gamma = \int \sum_\alpha |\dot{\gamma}_\alpha| dt. \tag{7}$$

The resolved shear stress, τ_α, is obtained as the projection of the symmetric second Piola–Kirchoff stress tensor $\boldsymbol{S}$ on the α slip system according to the expression:

$$\tau^\alpha = \boldsymbol{S} : \boldsymbol{s}^\alpha \otimes \boldsymbol{m}^\alpha = \boldsymbol{C} = \left[\frac{1}{2} (\boldsymbol{F}^{eT} \boldsymbol{F}^e) 1/2 - \boldsymbol{I} \right] : \boldsymbol{s}^\alpha \otimes \boldsymbol{m}^\alpha, \tag{8}$$

where $\boldsymbol{C}$ stands for the fourth-order elastic stiffness tensor of the crystal and $\boldsymbol{I}$ for the second-order identity tensor.

Finally, the Cauchy tensor, $\boldsymbol{\sigma}$, is calculated from the second Piola–Kirchoff tensor assuming small elastic deformations.

3.2. Finite-element simulations of indentations

The CP model described above was integrated into the finite-element (FE) commercial software ABAQUS [40] using a user material subroutine (UMAT). A three-dimensional FE model of the indentation process was generated. The model comprises a total of 10671 quadratic tetrahedral elements (C3D10M), using a refined mesh in the contact area. Individual grains were modeled as large cuboids so that the stresses at the borders could be neglected. The nodes at the bottom of the model were fully constrained. A fully rigid conical indenter was used in the simulations, assuming a tip radius of 50 nm. By inspection of the area function of the Berkovich tip used in the experiments, the apex angle of the conical tip used in the simulations was fixed at 71.2°. This is slightly larger than the theoretical apex angle (70.3°) of the conical tip that matches the area function of an ideal Berkovich tip, but ensures the one-to-one equivalency between the real indenter used in the experiments and the conical tip used in the simulations. The indenter was only allowed to move in the z direction. Since friction is known to play a minor role on the load vs. displacement response during indentation [41], frictionless contact was assumed between the rigid indenter and the material surface.

The following single-crystal elastic constants for Mg were used in all the simulations: C11 = 59.4 GPa,

C12 = 25.6 GPa, C13 = 21.4 GPa, C33 = 61.4 GPa and C44 = 16.4 GPa [10]. Due to the relatively low content of alloying elements, it was assumed that the elastic constants of the MN11 alloy are similar to those of pure Mg. Regarding the CP parameters, a total of 24 slip systems were considered, divided into four families (basal, prismatic, pyramidal ⟨a⟩, pyramidal ⟨c+a⟩), as summarized in Table 2. No twinning was considered, due to the small size of the experimental indentations, as justified in Section 4.3. In order to reduce the number of fitting parameters, the self-hardening and latent hardening parameters, $q_{\alpha\beta}$, were fixed to 1.0 for all the slip systems, so that only three parameters, namely the initial yield stress τ_0, the saturation yield stress, τ_s, and the initial hardening modulus h_0 were calculated. Moreover, a value of $1\ s^{-1}$ for the reference shear rate, $\dot{\gamma}_0$, was chosen in all cases. For each set of parameters, the hardness evolution with declination angle is determined from the calculated loading–unloading curves in the same fashion as the experimental curves, i.e. by the Oliver and Pharr method [35]. Finally, the CP parameters were optimized by fitting the simulated hardness–declination angle curves to the experimental ones.

4. Results and discussion

4.1. Indentation size effect in pure Mg

As mentioned in the Introduction, one of the main limitations in the use of nanoindentation tests as a calibration method for CPFEM models is the occurrence of the so-called ISE. It is well known that, in single-crystal metals, hardness increases as the indentation depth decreases [42–45]. The origin of this size effect is the increase in the plastic strain gradient that occurs for self-similar indenters with decreasing penetration depth [42]. This effect is particularly relevant at depths smaller than a few microns. This work aims at developing a universal method that can be applied to conventional polycrystalline Mg alloys with typical grain sizes of ~10 μm. As we aim at neglecting grain boundary effects, this results in the use of indentation depths <300 nm. However, at this indentation depth range, the ISE may be significant. This effect is typically explained in terms of geometrically necessary dislocations (GNDs) [44]. The hardness, H_{TOT}, is considered as the sum of two terms: a size-independent term, H_{SSD}, which depends on the density of statistically stored dislocations (SSD_s), and a size-dependent term, H_{GND}, related to the density of GNDs.

Table 2
Slip systems included in the crystal plasticity model.

	Slip plane	Slip direction	Number of systems
Basal	(0001)	$\langle 11\bar{2}0\rangle$	3
Prismatic	$\{10\bar{1}0\}$	$\langle 11\bar{2}0\rangle$	3
Pyramidal ⟨a⟩	$\{10\bar{1}1\}$	$\langle 11\bar{2}0\rangle$	6
Pyramidal ⟨c+a⟩	$\{10\bar{2}2\}$	$\langle 11\bar{2}3\rangle$	12

We have therefore evaluated the ISE in the current deformation conditions on pure Mg. Fig. 4 shows the variation of hardness with the indentation depth ranging between 100 and 3000 nm. This figure shows that hardness reaches a plateau corresponding to the size-independent term, H_{SSD}, at depths >2500 nm. At indentation depths of 300 nm, the hardness H_{300} shows a substantial size effect so that the size-dependent term H_{GND} accounts for 67% of the total hardness. Based on this result, a correction factor (CF) of 1.67 has been used in this work on the CPFEM calculations to estimate the size-independent hardness H_{SSD}, i.e. $H_{300} = H_{SSD} \times 1.67$. The use of a single CF parameter relies on the assumption that ISE is independent of grain orientation. Even though some authors [46] have reported that the accumulation of GNDs might be a function of grain orientation, our current studies show a similar ISE, so the same correction factor was assumed to be valid for all orientations.

4.2. Variation of the hardness with grain orientation

Figs. 2a and 3a show inverse pole figure (IPF) EBSD maps for both pure Mg (along the normal direction, ND) and the MN11 alloy (along the extrusion direction, ED), respectively. Several indentations were performed at the centre of selected grains in both materials. Fig. 2b shows the load vs. indentation depth curves corresponding to two grains, namely grain 1 and grain 2 in Fig. 2a, in pure Mg. Grain 1, with a declination angle of 2°, is significantly stronger than grain 2, which has a declination angle of 53°. Fig. 3b confirms that the mechanical response of individual grains in the MN11 alloy is also strongly affected by the grain orientation. In particular, grain 1, which has a small declination angle ($\delta = 7°$), is stronger than grain 2, which contains a higher declination angle ($\delta = 64°$).

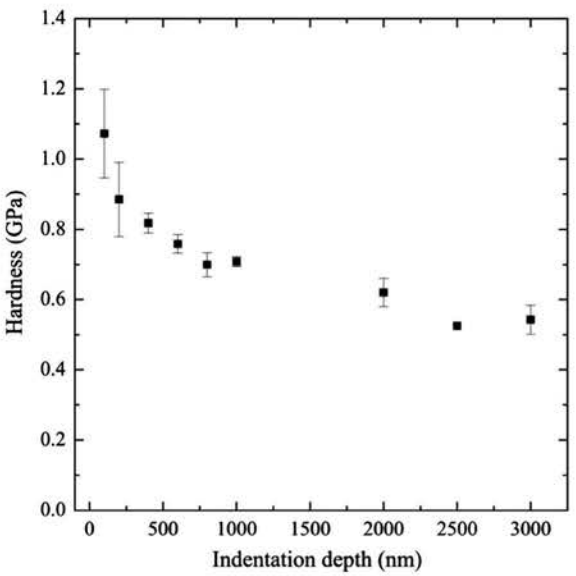

Fig. 4. Hardness vs. indentation depth curve corresponding to pure Mg.

Fig. 5 plots the variation of hardness with declination angle obtained for pure Mg and the MN11 alloy. While pure Mg exhibits a drop in the hardness at a declination angle ranging between 30° and 50°, the hardness drop takes place at a declination angle of 0–25° in the MN11 alloy. We ascribe this effect to the influence of grain orientation on the slip activity and the corresponding CRSS values.

4.3. Validation of the method for pure Mg

The parameters of the viscoplastic law were selected as those providing the best fit with the experimental curves. We set the reference strain rate to 1 s^{-1} and the strain-rate sensitivity, $n = 1/m$, to 33.33. To assess the validity of the approach, the indentation of pure Mg in different orientations was simulated using the CPFEM model described in Section 3.2. Table 3 summarizes the CP parameters (τ_0, τ_s and h_0) used for each slip system [10]. The agreement between the experimental and simulated hardness variation with grain orientation is reasonable (Fig. 6), considering that the CP parameters for pure Mg were taken from literature [10], without any fitting procedures. This indicates that the reported behavior is indeed a consequence of the different CRSS of each slip system in Mg and their different activity as a function of grain orientation with respect to the indentation axis.

Table 4 summarizes the cumulative activity of the different slip systems with the grain orientation obtained from the CPFEM simulations. The activation of basal slip was found to be almost independent of the declination angle δ. This is consistent with the fact that under the complex stress state that develops under the indent, basal slip is readily activated for all orientations due to its low CRSS. However, the harder pyramidal ⟨c+a⟩ and prismatic slip systems show opposite behaviors. While the activity of pyramidal ⟨c+a⟩ slip decreases with increasing δ, the activity of prismatic slip increases with it. This trend indicates that despite the complex stress state that develops under the indents, the activation of the harder slip systems, namely pyramidal and prismatic, is mostly governed by their Schmid factor with respect to the stress component parallel to the indentation direction. The grain orientation with the highest Schmid factor for pyramidal ⟨c+a⟩ slip is at $\delta = 0°$. We thus associate the high hardness values obtained in grains with basal orientation, i.e. $\delta = 0°$, to the activation of pyramidal slip. In particular, the ratio between the activity of pyramidal ⟨c+a⟩ and prismatic slip shows a maximum value of 2.10 at $\delta = 0°$ (basal orientation) and a minimum value of 0.28 at $\delta = 90°$ (prismatic

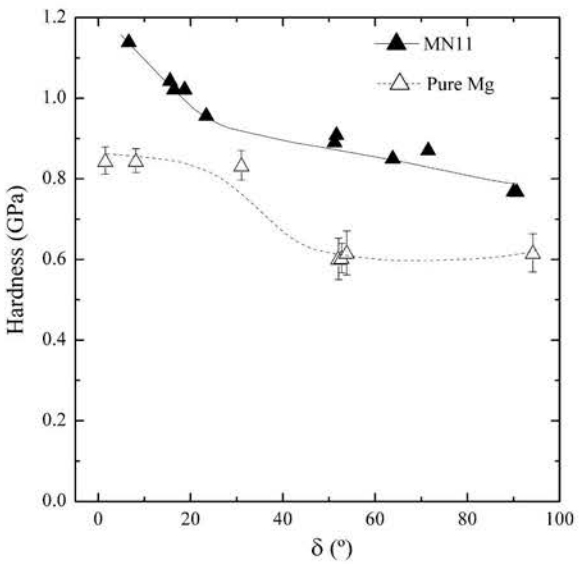

Fig. 5. Hardness vs. declination angle corresponding to pure Mg and to the MN11 alloy.

Table 3
Set of inelastic material parameters used in the validation of the model.

Slip system	τ_0	τ_s	h_0
Basal ⟨a⟩	2 (0.5)	10 (–)	20
Prismatic ⟨a⟩	25	85	1500
Pyramidal ⟨a⟩	25	85	1500
Pyramidal ⟨c+a⟩	40	150	3000

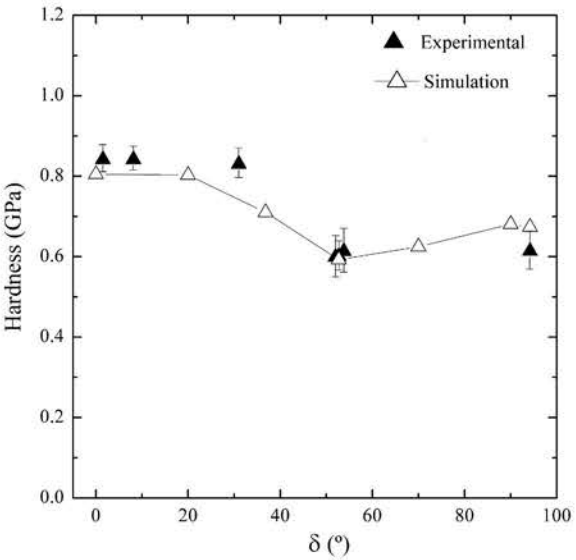

Fig. 6. Comparison between simulated and experimental hardness vs. declination angle curves for pure Mg.

Table 4
Slip system activity as a function of the declination angle during an indentation.

	Slip system activity (%)			
	Basal ⟨a⟩	Pris. ⟨a⟩	Pyra. ⟨a⟩	Pyra. ⟨c+a⟩
Declination angle (°)				
0	65	11	1	23
20	65	16	1	17
37	62	24	2	12
53	63	24	1	11
70	62	25	1	12
90	52	36	2	10

Table 5
Sets of CRSS values taken into account in the parametric study.

Set	τ_0 (τ_s)			
	Basal ⟨a⟩	Prismatic ⟨a⟩	Pyramidal ⟨a⟩	Pyramidal ⟨c+a⟩
1	25 (75)	25 (85)	25 (85)	25 (75)
2	5 (15)	5 (17)	25 (85)	40 (150)
3	3 (9)	24 (82)	15 (51)	24 (90)
4	3 (9)	25 (85)	25 (85)	40 (150)
5	3 (9)	37.5 (127.5)	25 (85)	40 (150)
6	3 (9)	3 (10)	37.5 (127.5)	60 (225)
7	3 (9)	37.5 (127.5)	37.5 (127.5)	60 (225)
8	3 (9)	60 (205)	37.5 (127.5)	60 (205)

orientation). Although pyramidal ⟨a⟩ slip was accounted for in the simulations, its activation was found to be negligible, in agreement with previous reports [47]. Finally, it is worth stressing that even though no twinning activity was considered in the CPFEM simulations of indentation in pure Mg, the agreement between experiments and simulations is remarkable. Tensile twinning is one of the softest deformation mechanisms in pure Mg and has actually been observed around large indentations (for depths >1 μm) both in this work and in previous studies [48]. However, careful examination of the surface around 300 nm deep indentations showed no evidence of twinning activity. Although the existence of nanotwins below the surface cannot be ruled out for very small indents, this observation indicates that deformation twinning has a negligible influence in the present deformation conditions. Interestingly, we observe an increase in the twinning activity with the indentation depth. This indicates the occurrence of an

Table 6
Simplifications assumed during the parametric study.

Parameter	Slip systems			
	Basal ⟨a⟩	Prismatic ⟨a⟩	Pyramidal ⟨a⟩	Pyramidal ⟨c+a⟩
h_0 (MPa)	20	1500	1500	3000
τ_s/τ_0 (except set 1)	3	3.4	3.4	3.75

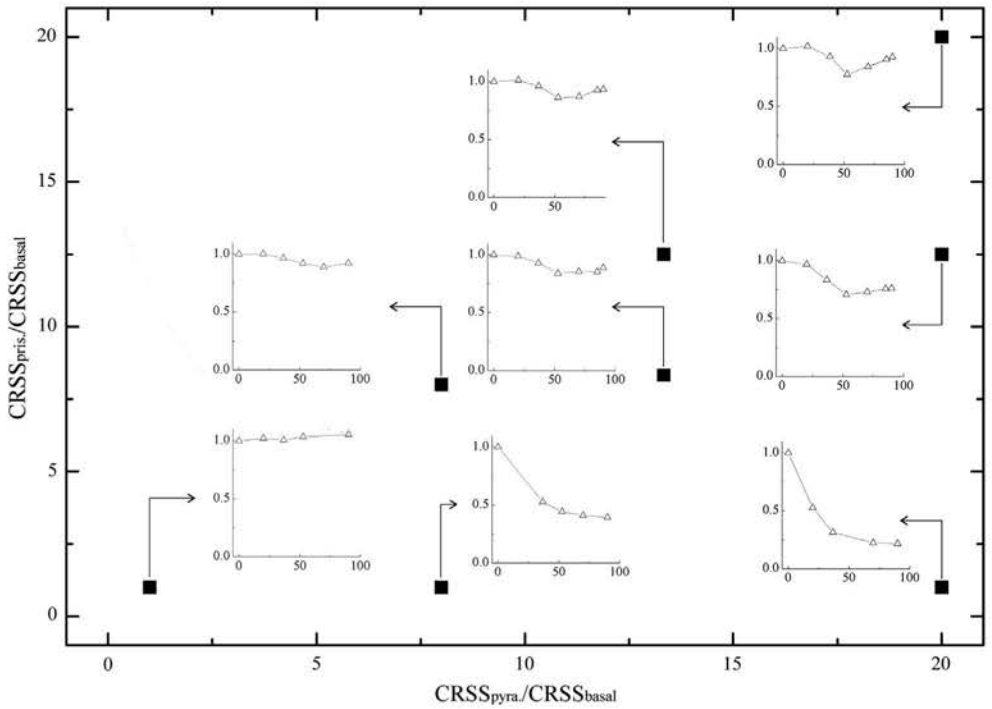

Fig. 7. Variation of the shape of the hardness vs. declination angle curve as a function of the ratios between the non-basal and the basal CRSS values.

ISE associated with the onset of twinning. This effect, which can be associated to the activation volume required for twinning [49–51], deserves further investigation.

4.4. Parametric study

Motivated by the success of reproducing the hardness variation with grain orientation in pure Mg, the CPFEM model was used to carry out a parametric study to assess the effect of the relative values of the different CRSSs on the hardness variation with grain orientation in Mg alloys. Eight different sets of CP parameters were considered, as summarized in Table 5. To minimize the number of parameters, a number of assumptions were made. First, the value of the initial hardening modulus of each slip system was set to that utilized in the validation study [10], Table 6. Second, the ratio τ_{sat}/τ_0 for each slip system was set to the values shown in Table 6 [10]. Third, the CRSS ratio between pyramidal ⟨c+a⟩ and pyramidal ⟨a⟩ slip was set to 1.6 [10]. Fourth, the strain-rate-sensitive exponent, $n = 1/m$, was set to 10. We allow variable τ_{sat}/τ_0 and CRSS ⟨c+a⟩/⟨a⟩ in one set of simulations, case 1 in Table 6. The variation in hardness with grain orientation for each set of parameters is summarized in Fig. 7 as a function of two parameters, namely, the pyramidal to basal CRSS ratio, $\tau_0^{pyr}/\tau_0^{basal}$, and the prismatic to basal CRSS ratio, $\tau_0^{prism}/\tau_0^{basal}$. For each set, all hardness values were normalized with respect to the hardness in the basal orientation, i.e. $\delta = 0°$.

The following conclusions can be drawn from Fig. 7. First, the pyramidal to basal CRSS ratio has a significant influence on the slope of the left branch of the H–δ curve, which becomes increasingly more negative as the $(\tau_0^{pyr}/\tau_0^{basal})$ ratio increases. This effect can be associated with the higher activation of pyramidal slip when the declination angle is small. On the other hand, the prismatic-to-basal CRSS ratio has a remarkable effect on the slope of the right branch of the curve, which increases with the increase of the $\tau_0^{prism}/\tau_0^{basal}$ ratio. Curves such as those shown in Fig. 7 can provide a qualitative assessment of the impact of alloying elements on the CRSS ratios of basal, prismatic and pyramidal slip in novel Mg alloys. Quantitative determination would require an optimization procedure of the simulated hardness to determine the CRSSs that best fit the experimental results, as shown below for the MN11 alloy.

4.5. Application of the method to an MN11 alloy

The H–δ curves obtained experimentally for pure Mg and for the MN11 alloy are shown in Fig. 5. The right branch of the curve for pure Mg displays a slightly positive slope, while the slope is negative for MN11. According to the previous parametric study, this trend is indicative of a reduction in the prismatic-to-basal CRSS ratio. This effect can be achieved by either increasing the basal CRSS, decreasing the prismatic CRSS, or a combination of both.

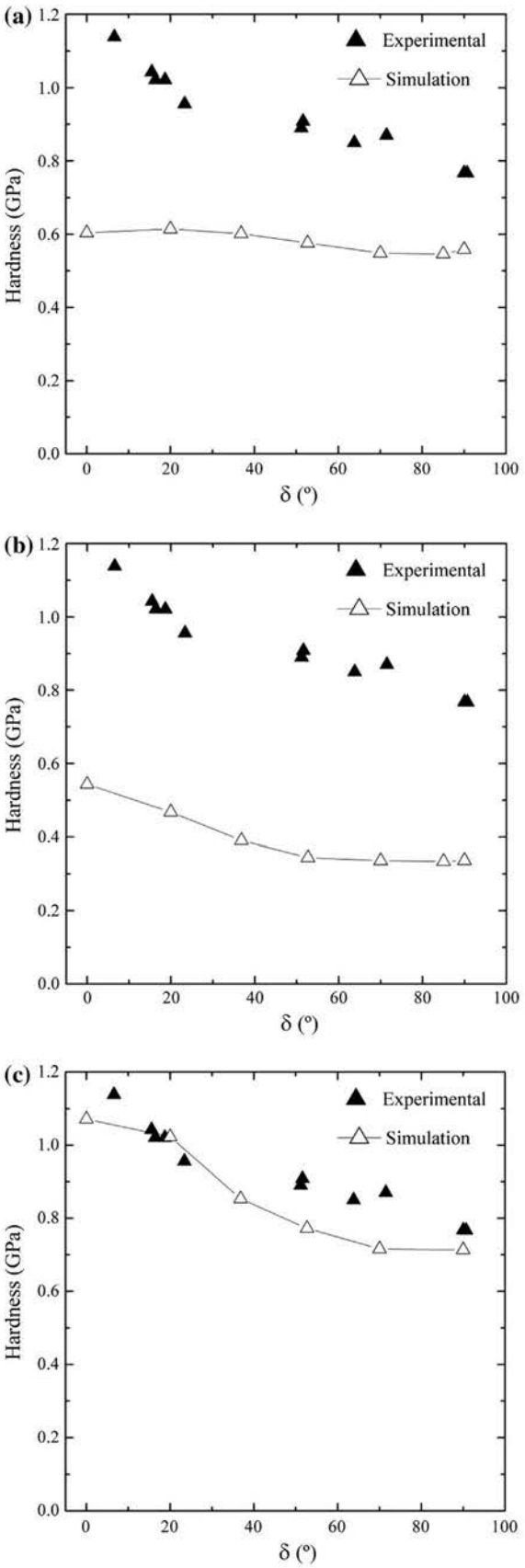

Fig. 8. Sets of CRSS values tested in order to match the experimental and simulated hardness vs. declination angle curves of the MN11 alloy: (a) increase in the basal CRSS; (b) decrease in the basal CRSS; (c) combination of an increase in the basal CRSS and a decrease in the prismatic CRSS.

Table 7
Set of CRSS values proposed for the MN11 alloy.

Slip system	τ_0	τ_s	h_0
Basal ⟨a⟩	35	105	20
Prismatic ⟨a⟩	20	80	1500
Pyramidal ⟨a⟩	60	300	1500
Pyramidal ⟨c+a⟩	95	345	3000

Fig. 8 reveals that increasing the basal CRSS (Fig. 8a) or decreasing the prismatic CRSS (Fig. 8b) independently leads to H–δ curves that differ widely from those measured experimentally. On the contrary, the experimental data are best matched by simultaneously increasing the basal CRSS, decreasing the prismatic CRSS and increasing the pyramidal ⟨c+a⟩ CRSS with respect to the values of pure Mg, as shown in Fig. 8c. The parameters that provide the best fit are summarized in Table 7.

The indentation results suggest that, while in pure Mg and conventional Mg alloys, such as AZ31, there is a large difference between the basal and prismatic CRSSs, in the case of the MN11 alloy, basal and prismatic slip display similar CRSSs. These results are consistent with previous reports that suggest softening of prismatic slip [24,52,53] and hardening of basal slip [23] in Mg upon alloying with RE elements. These differences in the CRSS between pure Mg and MN11 have been attributed to the presence of Nd in solid solution and to Mg_3Nd precipitates [23].

5. Conclusions

The main conclusions of this work can be summarized as follows:

1. A new methodology to estimate the CRSSs of the different slip systems in Mg alloys is proposed, which combines instrumented nanoindentation and CPFEM simulations, based on the variation of hardness with the crystallographic orientation of the grains.
2. The method was validated in pure Mg. We obtain a perfect match between the simulated and experimental variation of hardness with grain orientation, when adopting a set of published parameters measured recently by Zhang and Joshi in single crystals of pure Mg [10].
3. The CPFEM model was used to simulate the variation of hardness with grain orientation as a function of the CRSS ratios between non-basal and basal slip systems. The simulations show that the pyramidal to basal CRSS ratio is the most important parameter influencing the hardness of those grains oriented with the c-axis forming between 0° and 45° with the indentation axis. On the contrary, the prismatic to basal ratio influences mostly the hardness of those grains oriented with the c-axis forming between 45° and 90° with the indentation axis.
4. The proposed methodology was successfully used to estimate the CRSSs of the active slip systems in an extruded MN11 (Mg–1% Mn–1% Nd) alloy. It was found that, with respect to pure Mg, the basal CRSS increases dramatically and that the prismatic CRSS decreases, to an extent that both become similar. These variations in the CRSSs are consistent with previous experimental observations of the effect of Nd solutes and Mg_3Nd plate precipitates on slip activity, and are in agreement with the low yield stress anisotropy exhibited by these RE Mg alloys.

Acknowledgements

The authors wish to acknowledge financial support from the European Commission (ExoMet Project, 7th Framework Programme, Contract FP7-NMP3-LA-2012-280421) and from the Spanish Ministry of Economy and Competitiveness (MAT2012-31889). This investigation was also supported by the Spanish Ministry of Economy and Competitiveness (Projects PRI-PIBUS-2011-0990 and PRI-PIBUS-2011-0917) through the Materials World Network program.

References

Easton M, Beer A, Barnett M, Davies C, Dunlop G, Durandet Y, et al. J Met 2008;60:57.
Bamberger M, Dehm G. Annu Rev Mater Res 2008;38:505.
Schmid E. Z Elektrochem 1931;37:447.
Bakarian PW, Mathewson C. Trans AIME 1943;152:226.
Conrad H, Robertson W. Trans AIME 1957;209:503.
Reed-Hill R, Robertson W. Trans AIME 1957;496:496.
Ward PF, Mote J, Dorn J. Trans AIME 1961;221:1148.
Byer CM, Li B, Cao B, Ramesh KT. Scr Mater 2010;62:536.
Graff S, Brocks W, Steglich D. Int J Plast 2007;23:1957.
Zhang J, Joshi SP. J Mech Phys Solids 2012;60:945.
Christian JW, Mahajan S. Prog Mater Sci 1995;39:1.
Jin L, Dong J, Wang R, Peng LM. Mater Sci Eng A 2010;527:1970.
Bohlen J, Yi SB, Swiostek J, Letzig D, Brokmeier HG, Kainer KU. Scr Mater 2005;53:259.
Sadeghi A, Pekguleryuz M. Mater Sci Eng A 2011;528:1678.
Del Valle JA, Pérez-Prado MT, Ruano OA. Mater Sci Eng A 2003;355:68.
Styczynski A, Hartig C, Bohlen J, Letzig D. Scr Mater 2004;50:943.
Chino Y, Kimura K, Hakamada M, Mabuchi M. Mater Sci Eng A 2008;485:311.
Al-Samman T, Li X, Chowdhury SG. Mater Sci Eng A 2010;527:3450.
Ulacia I, Dudamell NV, Gálvez F, Yi S, Pérez-Prado MT, Hurtado I. Acta Mater 2010;58:2988.
Bohlen J, Nürnberg MR, Senn JW, Letzig D, Agnew SR. Acta Mater 2007;55:2101.
Mishra RK, Gupta AK, Rao PR, Sachdev AK, Kumar AM, Luo AA. Scr Mater 2008;59:562.
Bohlen J, Yi S, Letzig D, Kainer KU. Mater Sci Eng A 2010;527:7092.
Hidalgo-Manrique P, Yi SB, Bohlen J, Letzig D, Pérez-Prado MT. Metall Mater Trans A 2013;44:4819.
Robson JD, Twier AM, Lorimer GW, Rogers P. Mater Sci Eng A 2011;528:7247.
Sandlöbes S, Zaefferer S, Schestakow I, Yi S, Gonzalez-Martinez R. Acta Mater 2011;59:429.
Yasi JA, Hector Jr LG, Trinkle DR. Acta Mater 2011;59:5652.
Segurado J, Llorca J. Comput Mater Sci 2013;76:3.

Fernández A, Pérez Prado MT, Wei Y, Jérusalem A. Int J Plast 2011;27:1739.
Yoshinaga Y, Horiuchi R. Trans Jpn Inst Met 1963;4:134.
Hirsch P, Lally J. Philos Mag 1965;12:595.
Stanford N, Barnett MR. Int J Plast 2013;47:165.
Li H, Mason DE, Bieler TR, Boehlert CJ, Crimp MA. Acta Mater 2013;61:7555.
Herrera-Solaz V, Llorca J, Dogan E, Karaman I, Segurado J. Int J Plast 2014;57:1.
Qiao Y, Wang X, Liu Z, Wang E. Mater Sci Eng A 2013;568:202.
Oliver WC, Pharr GM. J Mater Res 1992;7:1564.
Lee EH. J Appl Mech 1969;36:1.
Peirce D, Asaro R, Needleman A. Acta Metall 1983;31:1951.
Asaro RJ, Needleman A. Acta Metall 1985;33:923.
Hutchinson JW. Proc Roy Soc Lond A 1976;348:1001.
ABAQUS/Standard V6.10 user's manual. ABAQUS Inc., Richmond, USA; 2009.
Bhattacharya AK, Nix WD. Int J Solids Struct 1988;24:881.
Pharr GM, Herbert EG, Gao Y. Annu Rev Mater Res 2010;40:271.
Hutchinson JW, Int J. Solids Struct 2000;37:225.
Nix WD, Gao H. J Mech Phys Solids 1998;46:411.
Poole WJ, Ashby MF, Fleck NA. Scr Mater 1996;34:559.
Britton TB, Liang H, Dunne FPE, Wilkinson AJ. Proc Roy Soc A: Math Phys Eng Sci 2010;466:695.
Bettles CJ, Barnett M. In: Bettles Colleen, Barnett Matthew, editors. Advances in wrought magnesium alloys: fundamentals of processing, properties and applications. Cambridge: Woodhead; 2012.
Shin JH, Kim SH, Ha TK, Oh KH, Choi IS, Han HN. Scr Mater 2013;68:483.
Lebensohn RA, Tomé CN. Philos Mag A 1993;67:187.
Zhang RY, Daymond MR, Holt RA. Mater Sci Eng A 2008;473:139.
Meyers MA, Vöhringer O, Lubarda VA. Acta Mater 2001;49:4025.
Tsuru T, Udagawa Y, Yamaguchi M, Itakura M, Kaburaki H, Kaji Y. J Phys: Condens Matter 2013;25:22202.
Chino Y, Kado M, Mabuchi M. Mater Sci Eng A 2008;494:343.